

Article

An Approach of Quantifying Gear Fatigue Life for Wind Turbine Gearboxes Using Supervisory Control and Data Acquisition Data

Yingning Qiu ^{1,*}, Lang Chen ¹, Yanhui Feng ¹ and Yili Xu ²

¹ School of Energy and Power Engineering, Nanjing University of Science and Technology, Nanjing 210094, China; chenlang4396@163.com (L.C.); Yanhui.feng@njust.edu.cn (Y.F.)

² Zhejiang Windey Ltd. by Share Ltd., 22F, Building A, the West Lake International Plaza S&T, No. 391, Wen'er Road, Hangzhou 310012, China; vanxuyili@sina.com

* Correspondence: yingning.qiu@njust.edu.cn; Tel.: +86-025-8431-7344

Received: 27 June 2017; Accepted: 21 July 2017; Published: 25 July 2017

Abstract: Quantifying wind turbine (WT) gearbox fatigue life is a critical problem for preventive maintenance when unsolved. This paper proposes a practical approach that uses ten minutes' average wind speed of Supervisory Control and Data Acquisition (SCADA) data to quantify a WT gearbox's gear fatigue life. Wind turbulence impacts on gearbox fatigue are studied thoroughly. Short-term fatigue assessment for the gearbox is then performed using linear fatigue theory by considering WT responses under external and internal excitation. The results shows that for a three stage gearbox, the sun gear in the first stage and pinions in the 2nd and 3rd stage are the most vulnerable parts. High mean wind speed, especially above the rated range, leads to a high risk of gearbox fatigue damage. Increase of wind turbulence may not increase fatigue damage as long as a WT has an instant response to external excitation. An approach of using SCADA data recorded every ten minutes to quantify gearbox long-term damages is presented. The calculation results show that the approach effectively presents gears' performance degradation by quantifying their fatigue damage. This is critical to improve WT reliability and meaningful for WT gearbox fatigue assessment theory. The result provides useful tools for future wind farm prognostic maintenance.

Keywords: wind turbine (WT); fatigue life; gearbox; supervisory control and data acquisition (SCADA) data

1. Introduction

The gearbox is an important mechanical component in a wind turbine (WT). Its availability and reliability attract attention due to the ultimate long downtime if it fails. The difficult accessibility of offshore wind farms further brings challenges to gearbox maintenance which requires an advanced operational and maintenance strategy for WTs [1,2]. Properly scheduled corrective and preventive maintenance both require effective WT fault detection, precise fault diagnosis and accurate prognosis techniques. To achieve efficient wind farm maintenance and competitive wind life-cycle cost, structural health monitoring techniques of WT system are being quickly developed through intelligent condition monitoring technique that integrates on-line fault detection and prognosis [3]. A model-based approach has been developed for WT gearbox fault detection [4]. Suitable methods and approaches are crucial for WT damage detection and fatigue accumulation estimation. Related technologies such as machine fatigue damage prognosis would greatly increase the value of condition monitoring in the drive train of WTs [5]. Different techniques have been developed for WT gearbox prognosis, which include using angular velocity measurements for bearing failure [6], hidden Markov models, neural networks and particle filter methods [7].

Currently, most WT gearbox designs are based on the ISO-6336 series [8] or IEC 61400 [9] in order to satisfy the minimum safety factors during the design stage. The question arises as to how to quantify WT's long-term fatigue life when they are operating under variable and turbulent wind conditions. In the standards only the short-term WT gearbox fatigue is considered [10]. Models and approaches to calculate WT gearbox long-term fatigue damage are developed based on linear fatigue theory and wind speed statistical distribution [10,11]. The most vulnerable components of the WT gearbox are compared and summarized to assist reliability-based maintenance [12]. The main reason for the randomness of fatigue damage lies in the characteristics of the material, the geometric dimensions of the test pieces, and the uncertainty of external loads [13]. Internal excitation can be considered by a detailed rigid and flexible multi-body model of a WT drive train which is normally used to study the internal dynamics of the mechanical transmission system [14–16]. However, external excitation of the gearbox coming from short-term scale rapid wind speed variation which is essentially correlated to wind turbulence effects attracts little research attention [17]. Irregular stress amplitudes of WT gearboxes due to WT's response to both external and internal excitation causes further complexity and difficulty for predicting gear damage and fatigue life. In addition, cost-effective gearbox damage quantification relies on a realistic measurement or implementation solution to enable the calculation.

Fatigue, wear or plastic deformation are common gearbox failure modes, of which the most common cause of gear failure is tooth bending fatigue [18]. Contact fatigue failure (pitting) and bending fatigue failure (tooth breakage) could be two of the main gear failure reasons [19]. Bending fatigue failure is a common failure mode in engineering and it happens when variable loads appear act a gear which leads to fatigue stress [20]. This paper is limited on studying bending stress fatigue analysis rather than micropitting and pitting fatigue life, that is bending stress is taken into account for gear fatigue life prediction without considering assembly errors and geometry defects.

This paper is focused on the mechanism of a gearbox's gear bending fatigue failure to develop a method to predict the fatigue life with practical supervisory control and data acquisition (SCADA) data. A dynamic model of the planetary gear system and a wind speed model that considers wind turbulence impacts is used. Time domain short-term WT gear meshing forces under different wind turbulence scales are obtained by a simulation model, which couples the WT model and the gearbox dynamic model. Load cycle distribution is then assessed for fatigue damage prediction based on linear fatigue damage theory. According to the low sampling rate characteristics of SCADA data, a practical approach is then proposed to quantify long-term gearbox gear fatigue damage, which is derived from the theoretical calculations and analysis results.

2. SCADA Data for Long Term Fatigue Quantification

The approach proposed in this paper to quantify WT gearbox is illustrated in Figure 1. Firstly, short-term gearbox damage under stochastic wind speed conditions is investigated by the calculation procedure shown in the left column in Figure 1. The short-term wind speed variation is characterized by the mean wind speed with different turbulence scale that represents the external excitation in the gearbox dynamics. The torque generated by the WT rotor is simulated by a fluid aerodynamic model, which is used as input of the drive train dynamic model. Internal excitation of WT gearbox is considered by taking varying meshing stiffness into account in calculating the time domain bending stress amplitudes. Stress cycles are counted by a rain-flow counting algorithm. As only the stress variation amplitudes are considered during cycle counting, Goodman corrections are adopted to account for the stress level influence. Finally, short-term fatigue damage of gears is obtained according to linear fatigue theory.

Secondly, a procedure of using SCADA data to quantify long-term damage of gearbox is presented. The WT SCADA data recorded ten minute average wind speeds and also the maximum and minimum values during this period. Accordingly wind turbulence scales within those ten minutes are calculated based on a mathematical derivation by assuming that the wind speed distribution is in accordance with statistics. This mathematical model is presented in Section 6. Corresponding short-term damage

quantification results are obtained, in terms of wind speed parameters, and then further accumulated for long-term damage quantification.

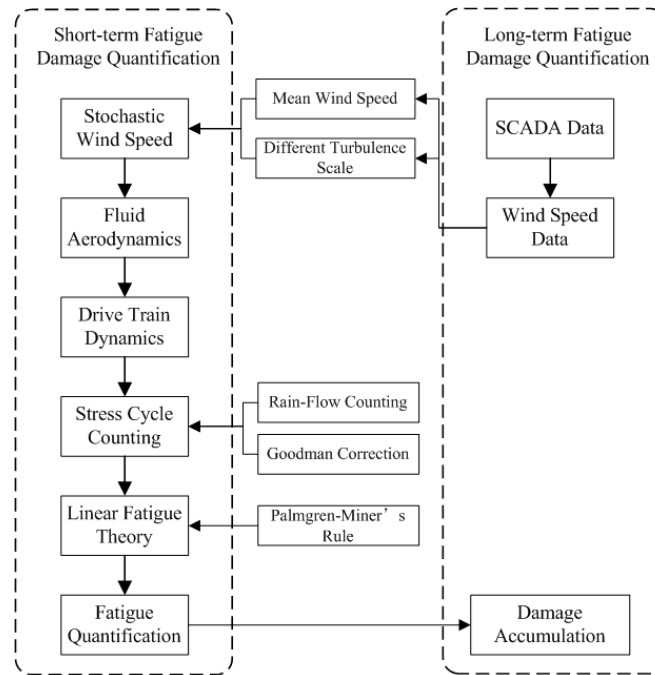


Figure 1. Flowchart of using supervisory control and data acquisition (SCADA) data to quantify gearbox gear fatigue damage.

Finally, a real case of using SCADA data to quantify gearbox damage is presented for a realistic WT that had suffered a catastrophic gear failure. It provides a cost-effective solution for gearbox damage quantification and performance monitoring from a practical point of view.

3. Wind Turbine Gearbox Stress Simulation

3.1. Wind Speed Simulation

In this paper, the external environment that a WT is subjected to refers to wind conditions only, which effects on WT loading are calculated. Short-term wind speed is characterized by the mean wind speed v_m and the turbulence-induced wind variation v_t during the statistical period, which can be expressed as:

$$v(t) = v_m(t) + v_t(t) \quad (1)$$

According to the WT cut-in and cut-out wind speed range, mean wind speeds from 4 to 25 m/s are considered [21]. A wind speed model that considers turbulence grades of A, B and C is constructed for a ten minutes period [17]. An improved Von Karman wind speed power spectrum model [22] is used to build the turbulence wind which takes air flow field into consideration for a thickness of the atmospheric boundary layer not exceeding 150 m. Accordingly, the longitudinal component of the auto-power spectral density function is shown in Equation (2). Equation (3) is the expression of the horizontal and vertical component of the auto-power spectral density:

$$\frac{f \cdot S_{uu}(f)}{\sigma_u^2} = \beta_1 \frac{2.987 \tilde{n}_u / a}{(1 + (2\pi \tilde{n}_u / a)^2)^{5/6}} + \beta_2 \frac{1.294 \tilde{n}_u / a}{(1 + (\pi \tilde{n}_u / a)^2)^{5/6}} F_1 \quad (2)$$

$$\frac{f \cdot S_{ii}(f)}{\sigma_i^2} = \beta_1 \frac{2.987(1 + (8/3)(2\pi \tilde{n}_i / a)^2)(\tilde{n}_i / a)}{(1 + (4\pi \tilde{n}_i / a)^2)^{11/6}} + \beta_2 \frac{1.294 \tilde{n}_i / a}{(1 + (\pi \tilde{n}_i / a)^2)^{5/6}} F_2 \quad (3)$$

where u is longitudinal dimension; \tilde{n}_u and \tilde{n}_i is dimensionless frequency parameters; f is frequency; $a, \beta_1, \beta_2, F_1, F_2$ are flow field parameters. GH Bladed software (GL Garrad Hassan, Hamburg, Germany) was used to produce ten minute wind speed data with an improved Von Karman wind speed power spectrum model [23].

3.2. Wind Turbine Drive Train Principle

Random wind speeds caused WT variable loads are obtained by simulation. According to aerodynamics theory, the power that is produced by the wind can be expressed as:

$$P_m = \frac{\pi}{2} C_p \rho R^2 v^3(t) \quad (4)$$

where P_m (W) is the WT output power (transmission input power); C_p is the efficiency factor; ρ (kg/m^3) is the air density; R (m) is the rotor radius; v (m/s) is wind speed.

T_m , which is the torque of main shaft, can be calculated with the following equations:

$$\lambda = \frac{\omega_r R}{v} \quad (5)$$

$$T_m = \frac{P_m}{\omega_r} = \frac{1}{2} \rho \pi R^3 v^2(t) C_p / \lambda \quad (6)$$

where ω_r (rad/s) is the angular velocity of wind wheel; λ is the tip speed ratio.

Rotational speed and torque of the rotor generated under turbulence wind speeds are the input of the gearbox dynamic model to obtain the force and moment of gear meshing.

3.3. Gearbox Dynamic Model

The WT gearbox being considered is a three-stage gearbox as shown in Figure 2. It is composed by a planetary helical stage and two parallel helical stages. WT rotor's mechanical torque is transmitted through the gearbox to the generator. A three-stage gearbox dynamic model [24] is established with the assumption of a uniform arrangement of three planet gears with the same geometrical parameters. The mesh between gear pairs is considered as a spring with time-varying stiffness and gear damping. The gears' comprehensive engagement error is not considered here. A three-stage gearbox that is being treated as a lumped mass torsional model is shown in Figure 3, in which k represents gear meshing stiffness, c represents the meshing damping of gear pair, θ represents the angle of gear rotation, J represents the rotational inertia of gear, and T represents the gear torque.

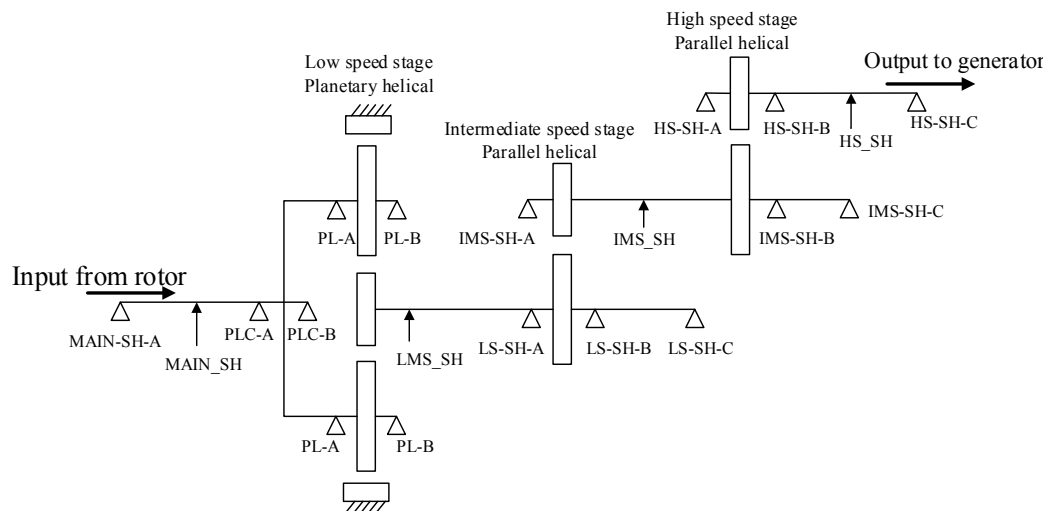


Figure 2. The topology of the gearbox.

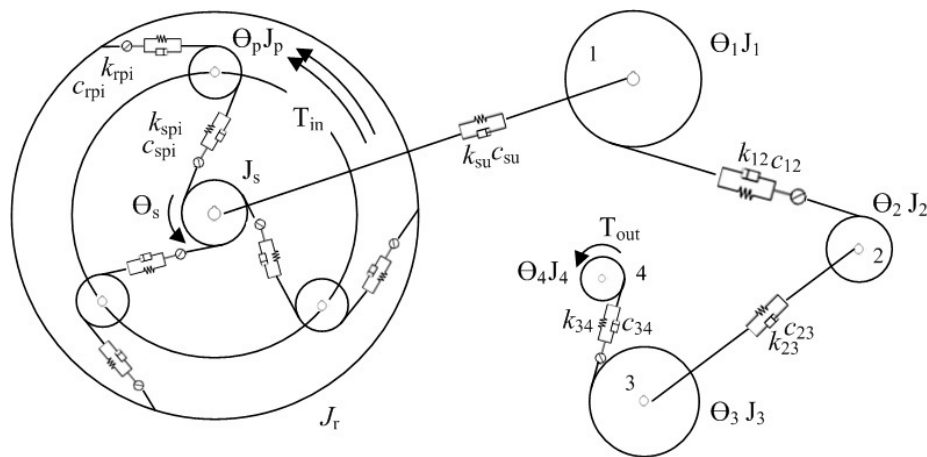


Figure 3. Dynamic model of the three-stage gearbox.

In the multibody simulation method, the gearbox is modeled as an interconnection of a number of flexible bodies. The motion of the drive train can be expressed in Lagrange formalism:

$$M\ddot{q} + C\dot{q} + Kq = F \quad (7)$$

where M is the generalized mass matrix, q is the vector of the degrees of freedom, K is the varying gear meshing stiffness matrix, C is the varying gear meshing damping matrix, F is the excitation of a gear pair. This paper established a three-stage gearbox dynamic model based on the Lagrange formalism equation of gear pairs with a unified coordinate system. The dynamic equations of planetary stage of gearbox are shown below:

$$\left\{ \begin{array}{l} (I_c/r_c^2 + Nm_p)\ddot{u}_c + k_{ct}u_c + c_{ct}\dot{u}_c + k_{cu}u_c + c_{cu}\dot{u}_c = \\ \sum_{i=1}^N (F_{spi}\cos\alpha_s + F_{rpi}\cos\alpha_r) + T_{in}/r_c \\ (I_r/r_r^2)\ddot{u}_r + k_{rt}u_r + c_{rt}\dot{u}_r = \sum_{i=1}^N (-F_{rpi}) \\ (I_s/r_s^2)\ddot{u}_s + k_{st}u_s + c_{st}\dot{u}_s + k_{st}(u_s - u_1) + c_{st}(\dot{u}_s - \dot{u}_1) = \sum_{i=1}^N (-F_{spi}) \\ (I_{pi}/r_{pi}^2)\ddot{u}_{pi} = (F_{rpi} - F_{spi}) \\ F_{spi} = k_{spi}\delta_{spi} + c_{spi}\dot{\delta}_{spi} \\ F_{rpi} = k_{rpi}\delta_{rpi} + c_{rpi}\dot{\delta}_{rpi} \end{array} \right. \quad (8)$$

where N is the number of planet, m_p is the mass of planet, T_{in} is the torque of planetary carrier. J , r , u is the rotational inertia, the base circle radius and torsional displacement in the unified coordinate respectively. Their subscribes of c , r , s and pi are referring to planet carrier, ring, sun and planet ($i = 1, 2, 3$) individually. k_{ct} , k_{rt} , k_{st} , k_{cu} are the tangential bearing stiffness of planetary carrier, ring, sun and the torsional stiffness of planetary carrier shaft, c_{ct} , c_{rt} , c_{st} , c_{cu} are the tangential bearing damping of planetary carrier, ring, sun and the torsional damping of planetary carrier shaft, k_{rpi} , c_{rpi} , F_{rpi} , α_r are the meshing stiffness, meshing damping, meshing force and angle of engagement between ring and planet, k_{spi} , c_{spi} , F_{spi} , α_s are the meshing stiffness, meshing damping, meshing force and angle of engagement between sun and planet, δ_{spi} , δ_{rpi} are the projection of the displacement of the sun and the ring in the direction of external meshing line while the planet are assumed to be immobile.

The Newmark method is used for the time integration of the dynamic equations of gearbox [25–27]. Its procedure to solve the dynamic model is listed below:

Calculate the matrix of stiffness K , dumping C and mass M for the multibody dynamics system of gearbox.

Set initial value of $U_0, \dot{U}_0, \ddot{U}_0, \Delta t, \gamma, \sigma$, calculating integral constant:

$$\begin{cases} \gamma \geq 0.5, \delta \geq 0.25(0.5 + \gamma)^2 \\ a_0 = \frac{1}{\delta \Delta t^2}, a_1 = \frac{\gamma}{\delta \Delta t} \\ a_2 = \frac{1}{\delta \Delta t}, a_3 = \frac{1}{2\delta} - 1 \\ a_4 = \frac{\gamma}{\delta} - 1, a_5 = \frac{\Delta t}{2}(\frac{\gamma}{\delta} - 2) \\ a_6 = \Delta t(1 - \gamma), a_7 = \gamma \Delta t \end{cases} \quad (9)$$

Obtain the matrix equivalent stiffness \bar{K} :

$$\bar{K} = K + a_0 M + C \quad (10)$$

and get the $U_{t+\Delta t}, \dot{U}_{t+\Delta t}, \ddot{U}_{t+\Delta t}$:

$$\begin{cases} \bar{Q}_{t+\Delta t} = Q_t + M(a_6 \dot{u}_t + a_2 \ddot{u}_t + a_3 \ddot{u}_t) + C(a_1 u_t + a_4 \dot{u}_t + a_5 \ddot{u}_t) \\ \bar{K} u_{t+\Delta t} = (LDL^T) u_{t+\Delta t} = \bar{Q}_{t+\Delta t} \\ \ddot{u}_{t+\Delta t} = a_0 (u_{t+\Delta t} - u_t) - a_2 \dot{u}_t - a_3 \ddot{u}_t \\ \dot{u}_{t+\Delta t} = \dot{u}_t + a_6 u_t + a_7 \ddot{u}_{t+\Delta t} \end{cases} \quad (11)$$

where the $\Delta t = 0.1s, \gamma = 0.5, \sigma = 0.25$ in this paper.

3.4. Gearbox Internal Excitation

Gearbox internal excitation is essentially due to variation of the meshing stiffness. Time-varying gear meshing stiffness is considered and approximated in accordance with the Ishikawa method [28], which uses Fourier series expansion and omits higher-order terms:

$$k = k_{\min} + (k_{\max} - k_{\min})(e - 1) + \sum_{i=1}^{\infty} \frac{k_{\max} - k_{\min}}{i\pi} [\sin 2\pi i(\gamma + e - 1 - \frac{t}{T}) - \sin 2\pi i(\gamma - \frac{t}{T})] \quad (12)$$

where k_{\max} is the meshing stiffness with two pair of teeth, k_{\min} is the meshing stiffness with one pair of teeth, T is the meshing period, γ is the phase angle, e is the contact ratio.

The gear meshing damping is also time-varying which is:

$$c = 2\xi_m \sqrt{\frac{kR_1^2 R_2^2 J_1 J_2}{R_1^2 J_2 + R_2^2 J_1}} \quad (13)$$

where ξ_m is the damping ratio. Its value is in the range of 0.03~0.17, k is the time-varying gear meshing stiffness, R is the radius of base circle of gear and J is the rotational inertia of gear.

Combining the three parts of the gearbox dynamics model, the load spectrum of a single gear can be obtained. According to ISO 6336:3-1996 [29] and GB/T3480-1997 [30], gear tooth root bending stress is calculated as:

$$\sigma_F = \frac{F_t}{bm_n} Y_{Fa} Y_{Sa} Y_{\epsilon} Y_{\beta} K_V K_{F\alpha} K_{F\beta} \quad (14)$$

where σ_F is tooth root bending stress; F_t is tangential force; b is the tooth width; m_n is the modulus; Y_{Fa} , Y_{Sa} is shape factor; Y_{ϵ} is the superposition degree modulus; Y_{β} is helix angle factor; K_V is the dynamic load factor; $K_{F\beta}$ is tooth surface load factor; $K_{F\alpha}$ is tangential load factor.

4. Wind Turbine Short-Term Fatigue Damage Quantification

WT gears are subjected to irregular stress which is due to its unique external condition of random and turbulent wind. This is an irregular random process, in which the magnitude of the random variable loads, fatigue damage estimation and service life time prediction are complex. Fatigue

damage estimation of gears is performed by tooth root bending stress cycle counting, which essentially assumes that failure mechanism of a gear is a cumulative process. Normally this is calculated by Palmgren-Miner's linear damage rule [31].

The rain-flow (RF) cycle method [32] assumes that the plasticity of materials results in fatigue damage which can be reflected on the stress-strain hysteresis loop. The rain-flow cycle algorithm records the amplitude and means value of the stress, so that it obtains all the information of the stress cycle of the material. A full RF cycle [33] was defined as a stress range formed by two points which are bounded within adjacent points of higher and lower magnitude.

The Palmgren-Miner theory is based on two assumptions: (1) the materials' fatigue damages under different stress levels are independent of each other; (2) the materials fatigue damage can be linearly accumulative. Damage is calculated with Equation (15):

$$\sum_1^m \frac{n_i}{N_i} = \frac{n_1}{N_1} + \frac{n_2}{N_2} + \frac{n_3}{N_3} + \frac{n_4}{N_4} + \dots + \frac{n_m}{N_m} = D \quad (15)$$

Stress cycle are counted by the rain-flow cycle method and its amplitude should be normalized to a zero-mean stress level before applying the Palmgren-Miner theory. When the critical value D of linear cumulative fatigue damage approaches 1, the theory predicts the material is broken. In this process, as only the cycles with the same stress variation amplitude are counted for the full cycles, the influences of mean stress values actually are not reflected in the rain flow counting process. To consider the mean stress value effects, a Goodman linear equation is used to calculate equivalent loads as shown in Equation (16) [34]:

$$\sigma_{ea} = \frac{\sigma_b \sigma_a}{\sigma_b - \sigma_m} \quad (16)$$

where σ_{ea} is the zero-mean equivalent stress level; σ_b is stress limit of material; σ_a is the amplitude of stress; σ_m is the mean stress. Using Goodman equation asymmetric stress levels are transformed into symmetric stress (zero-mean) levels.

5. Simulation

This paper studies a WT with rated power of 1.5–2 MW. The design parameters of the WT include: rotor diameter of 79.2 m, air density of 1.225 kg/m³, the tip speed ratio of 6.3, wind energy utilization coefficient of 0.32. The WT configuration parameters are listed in Table 1 and the gearbox geometry parameters are listed in Table 2. The calculation is for a WT which has failed during operation due to broken teeth observed in the planetary stage gears.

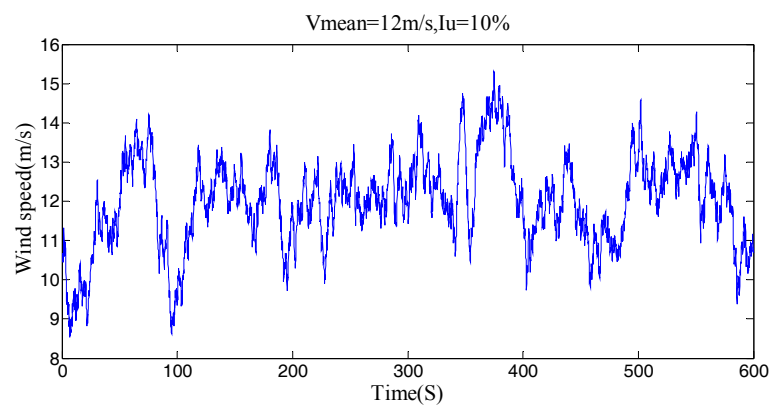
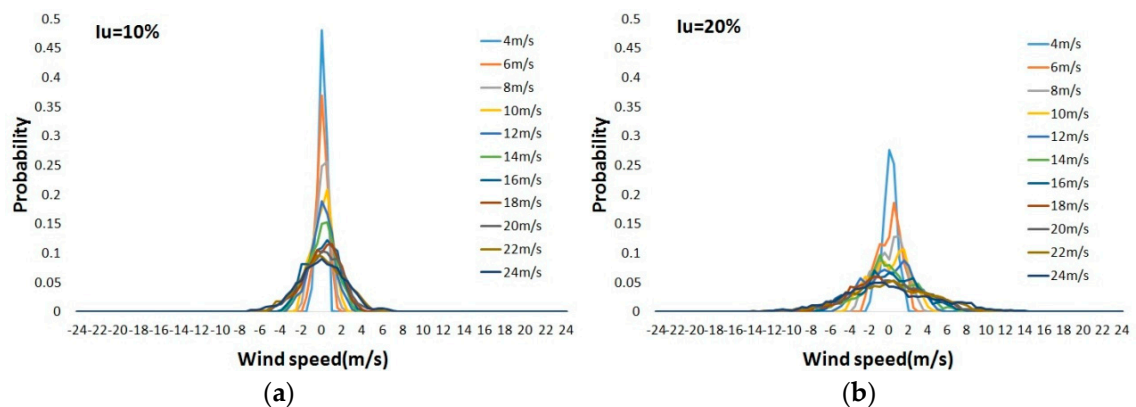
Table 1. Wind turbine (WT) technical parameters.

Parameters	Values
Cut-in Wind Speed	4 m/s
Cut-out Wind Speed	25 m/s
Rated Wind Speed	12 m/s
Hub Height	70 m
Rotor Diameter	79.2
Control Mode	Pitch Control

For demonstration purposes, the time domain wind speed variation with a mean wind speed of 12 m/s and turbulence intensity of 10% generated by the GH Bladed software is shown in Figure 4. Normalized wind speed statistical distributions for different mean wind speeds at different turbulence scales of 10%, 20% and 30% are plotted in Figure 5. It shows that with the increase of the wind turbulence intensity the 10 min wind speed statistical distribution covers a wider range, which essentially presents a wider range of wind speed variation.

Table 2. Gearbox's geometry parameters.

Stages	Parameters	Planet Carrier	Ring	Sun	Planet
Planetary stage	mass (kg)	515.4	114.1	379.7	187.6
	rotational inertia	1873.9	158.32	14.7	26.06
	radius of gear base circle (mm)	696	1160	232	464
	Number of teeth	-	145	29	58
	modulus		16		
	angle of engagement		20		
Stages	Parameters	Helical Gear1		Helical Gear2	
Middle stage	mass (kg)	1921.3		118.3	
	rotational inertia	556.8		2.2	
	radius of gear base circle (mm)	648		162	
	Number of teeth	108		27	
	modulus			12	
	angle of engagement			20	
Stages	Parameters	Helical Gear3		Helical Gear4	
High speed stage	mass (kg)	701.7		44.7	
	rotational inertia	136		0.5	
	radius of gear base circle (mm)	515		78	
	Number of teeth	103		25	
	modulus			10	
	angle of engagement			20	

**Figure 4.** Turbulent wind speed.**Figure 5.** Cont.

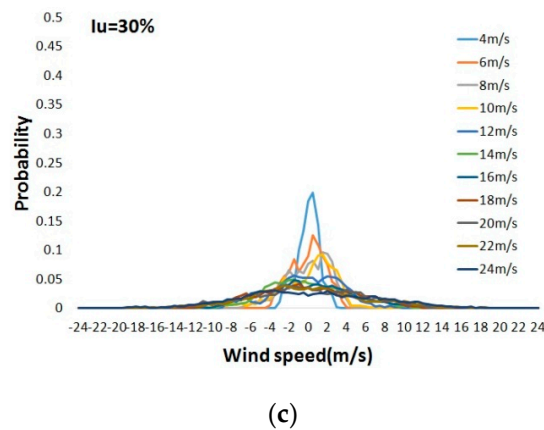


Figure 5. Normalized wind speed distribution with different turbulence scales: (a) 10%; (b) 20%; (c) 30%.

With 10% wind turbulence scale, the WT aerodynamic torques of the main shaft in response to different external wind conditions are shown in Figure 6a,b. Figure 6a shows the torque variation of the WT main shaft under wind speeds from 4 to 10 m/s (under the rated wind speed range). The torques' magnitudes increase with the increase of mean wind speed under this situation. Figure 6b shows its variation under wind speeds from 10 to 22 m/s (above the rated wind speed range). When the wind speed is below the rated range, the WT controls the rotational speed to maintain maximum output power. When the wind speed is above the rated range, the WT controls the blade pitch angle to maintain constant output power. Therefore, when the wind speed is above the rated range as shown in Figure 6a,b, the torques' magnitudes are maintained due to the constant output power and rotational speed under the WT's constant speed control mode. However, there are sudden drops of torque magnitudes for the high mean wind speed condition which is when the wind speed is above the cut-out range, as shown in Figure 6c,d. Under this situation, the WT stops operating. Figure 7 shows the statistical result of the main shaft torque for varying mean wind speed and wind turbulence intensity. It shows that when the mean wind speed is below the rated range the main shaft torque values increase with the increase of mean wind speed. When the wind turbulence intensity increases the main shaft torques' variation magnitudes increase, while when the mean wind speed is above the rated range, the main shaft torques remain constant.

The meshing force and bending stress between the planetary gear and sun gear calculated by the multi-body dynamics model of the gearbox are shown in Figure 8. The results of two cases are shown individually for wind speeds below and above the rated range. It shows that due to the gear meshing process, the meshing force exhibits obvious periodical features. The mean meshing force increases when the wind speed is below the rated range while it remains constant when the wind speed is above the rated range. The variation amplitude of meshing forces are higher for wind speeds above the rated range compared to the case where the wind speed is below the rated range. Its statistical results, as shown in Figure 9, indicate that with the increases of turbulence intensities the meshing force variation covers a wider range at the below rated wind speed range while they exhibit a similar distribution at above the rated wind speed range. The negative meshing forces observed in Figures 8 and 9 are due to the force direction variation.

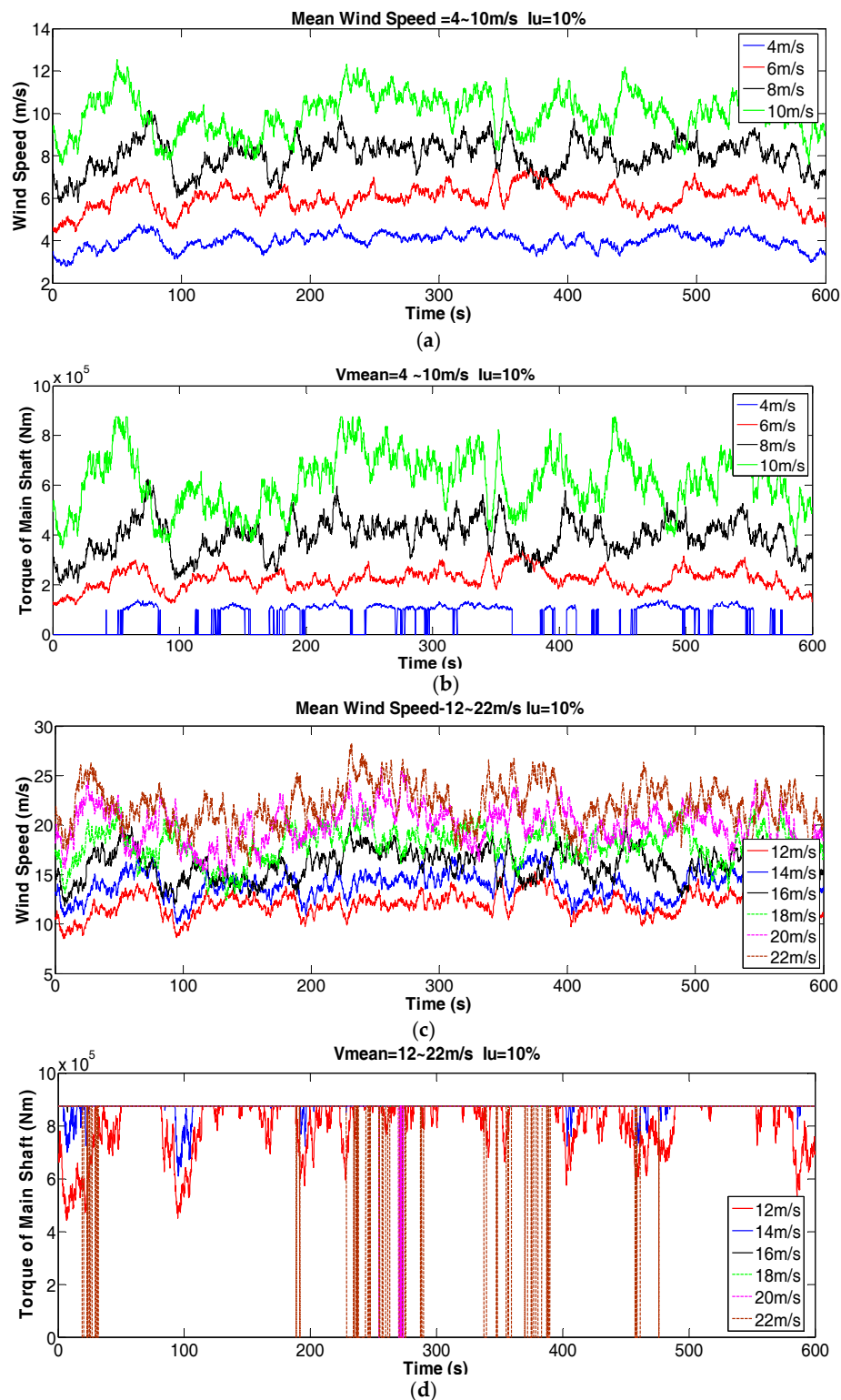


Figure 6. Time domain: (a) wind speed with mean value = 4–10 m/s, $I_u = 10\%$; (b) corresponding torque of main shaft; (c) wind speed with mean value = 12–22 m/s, $I_u = 10\%$; (d) corresponding torque of main shaft.

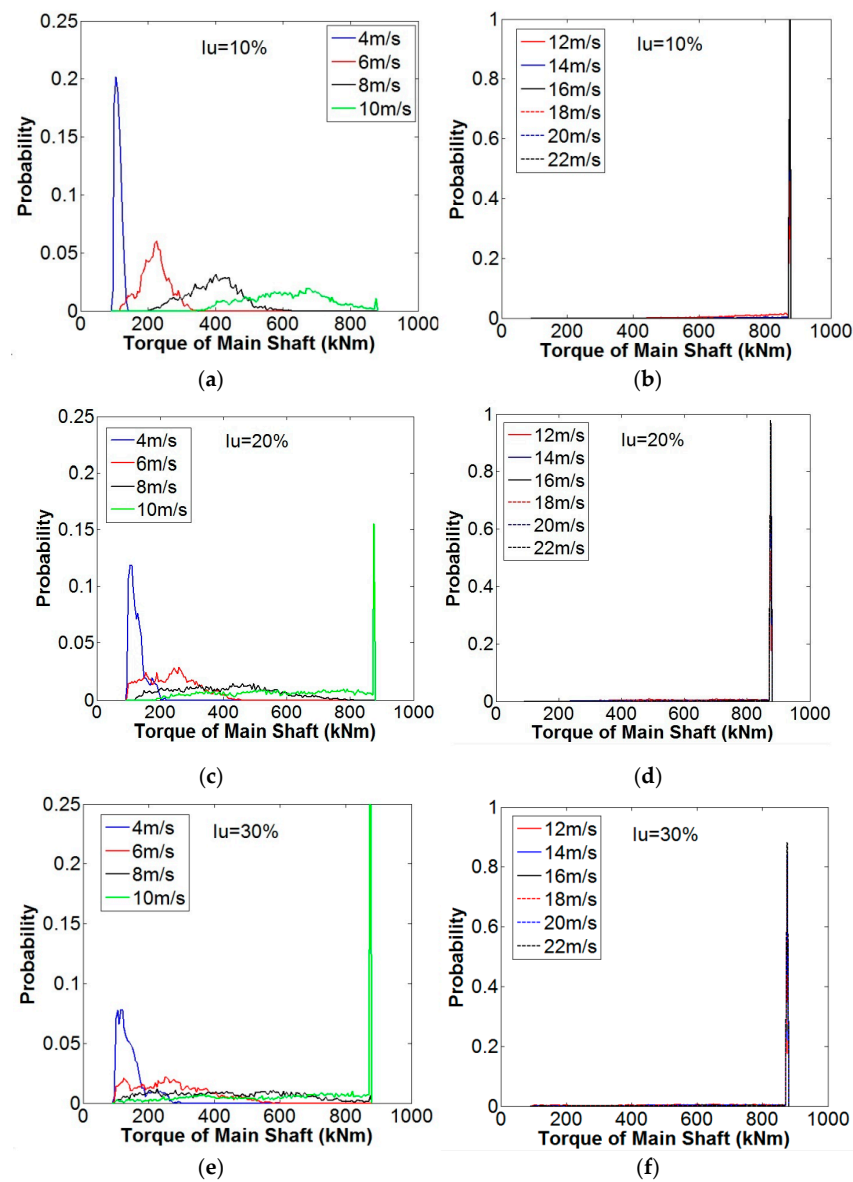


Figure 7. Statistics of WT main shaft's torques of mean wind speeds varying from 4 to 22 m/s: (a,b) 10%; (c,d) 20%; (e,f) 30%.

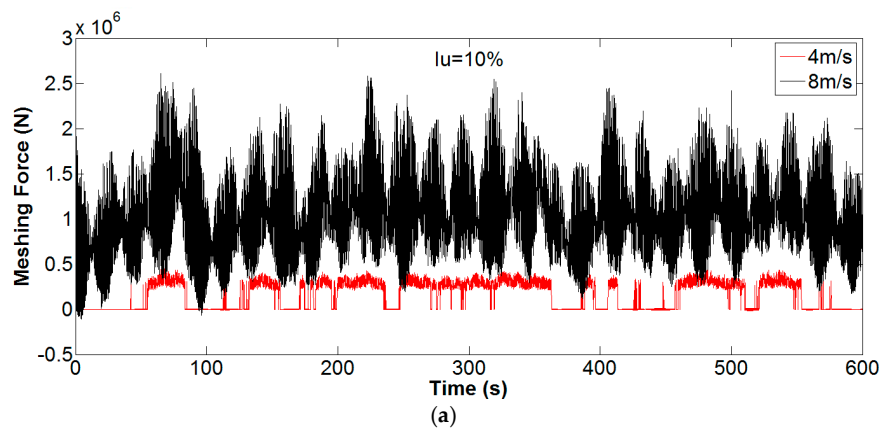


Figure 8. Cont.

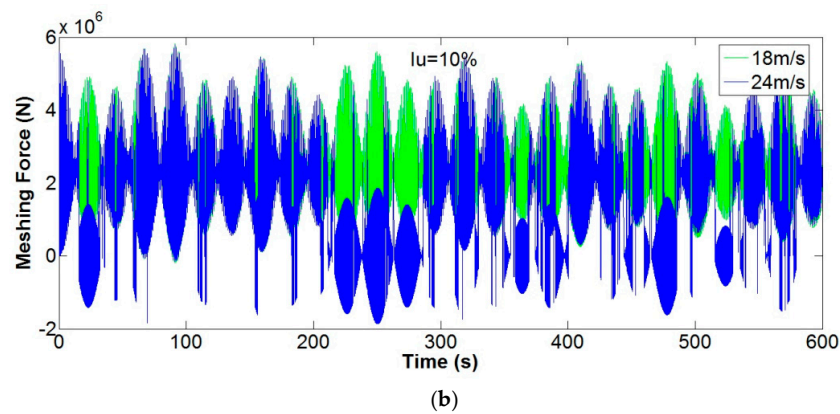


Figure 8. The meshing force between planetary gear and sun gear: (a) is for wind speed of 4 and 8 m/s; (b) is for wind speed of 18 and 24 m/s.

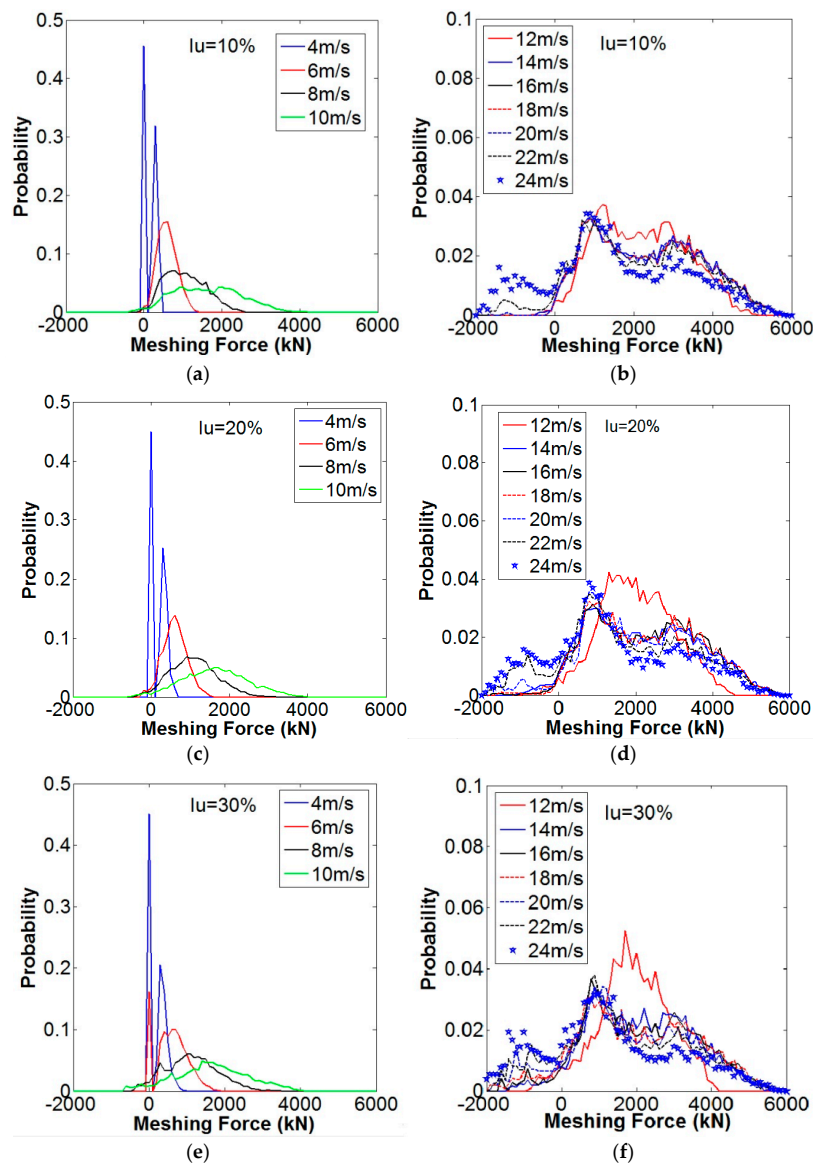


Figure 9. Distribution of meshing forces between planetary gear and sun gear for mean wind speeds varying from 4 to 24 m/s with different wind turbulence intensities. (a,b) 10%; (c,d) 20%; (e,f) 30%.

The calculated bending stress of the sun gear is shown in Figure 10. This bending stress shows a similar variation of meshing force as observed in Figure 9.

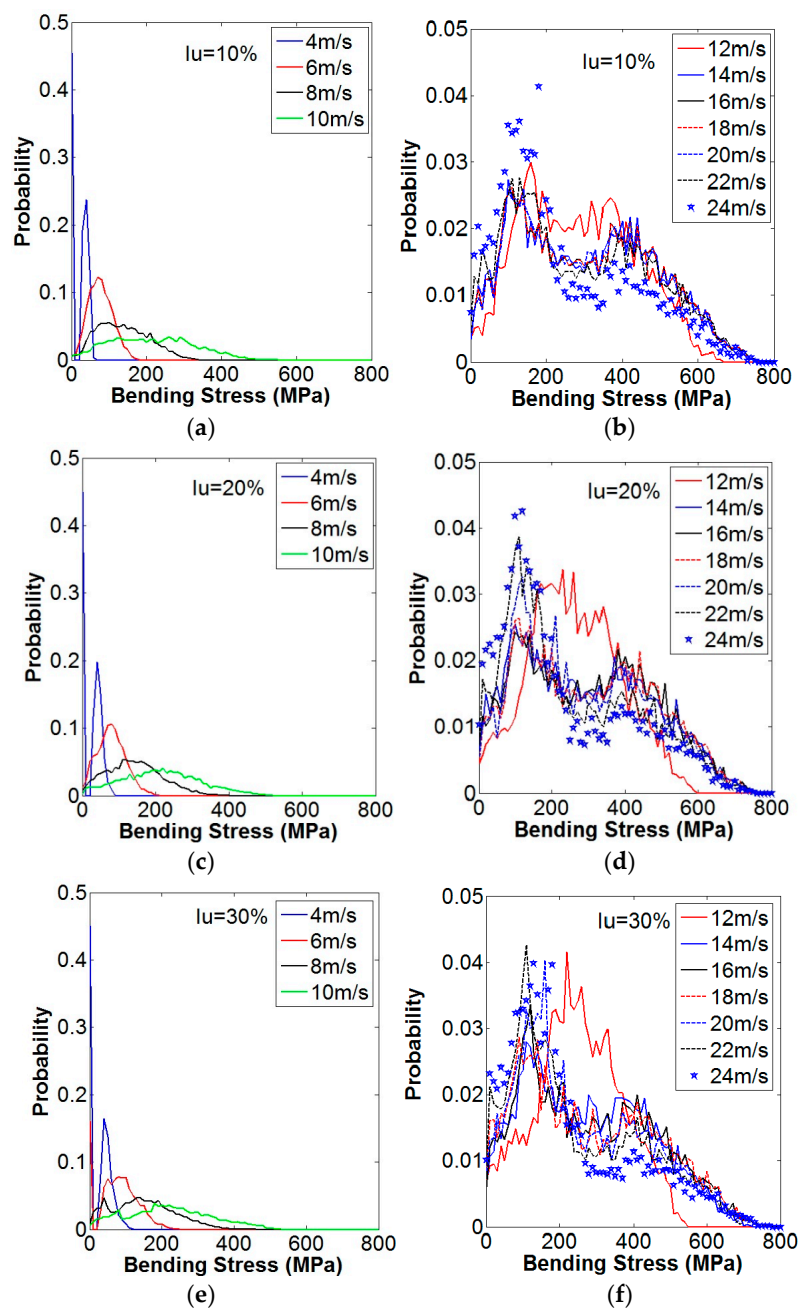


Figure 10. Bending stress of sun gear for wind speeds varying from 4 to 24 m/s with different turbulence intensities: (a,b) 10%; (c,d) 20%; (e,f) 30%.

Figure 11 shows the rain-flow counting results of mean wind speeds of 8 and 12 m/s. It shows that for mean wind speeds of 8 and 12 m/s the mean and amplitude of the bending stress between the planetary gear and sun gear are both in the range of 0–300 MPa. Bending stress is the main cause of gearbox fatigue damage.

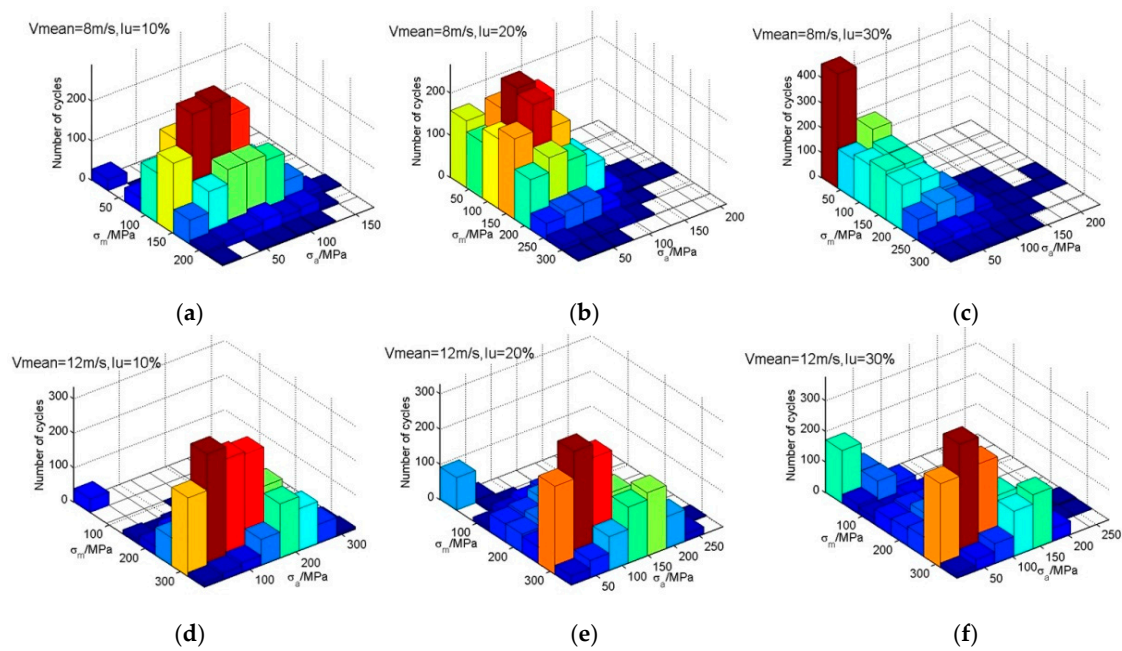


Figure 11. The bending stress between planetary gear and sun gear of 8 m/s with different turbulence intensities: (a) 10%; (b) 20%; (c) 30% and that of 12 m/s with different turbulence intensities: (d) 10%; (e) 20% and (f) 30%.

Figure 12 shows the probability of the sun gear's bending stress amplitude after Goodman correction. It shows that the probability of large bending stress amplitudes decrease with the increase of wind turbulence intensities. With the increase of mean wind speed ($v = 12\text{ m/s}$) an increase of probability of the large bending stress amplitudes is observed.

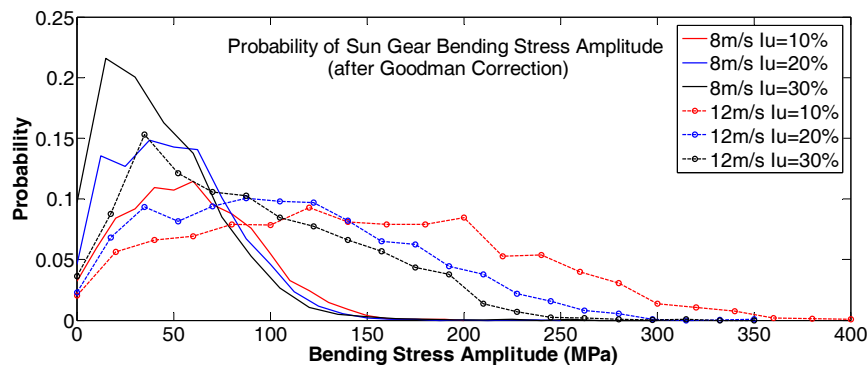


Figure 12. Probability of sun gear bending stress amplitude after Goodman correction.

Figure 13 shows the calculated result of gearbox fatigue damage under stochastic external excitation within 10 min. In each subfigures it shows the damage quantification result for the same turbulence scale with mean wind speeds ranging from 4 to 25 m/s. It is observed that the most vulnerable part within a gearbox is the sun gear, which shows greater damage than other components under the same conditions. For the second and third stages of a WT gearbox, the pinions are more vulnerable than gears. The results show significant differences in short-term fatigue damage at different gearbox stages for the case of mean wind speeds above 10 m/s in 10 min. The fatigue damage of different gearbox stages increases with the increase of wind turbulence scale while their tendencies are similar. A sharp increase of damage occurs when the wind speeds are above the rated range, which is

due to the increased probability of the bending stress amplitude (in Figure 12) which comes from large bending stress variation amplitude (in Figure 10).

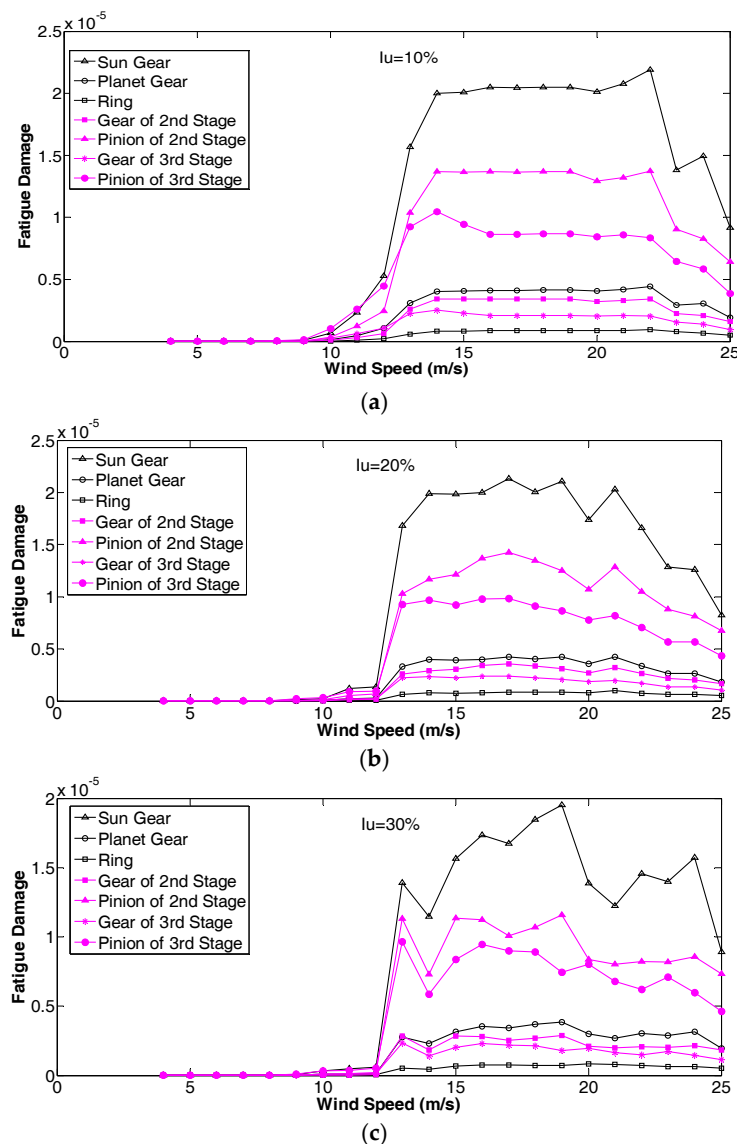


Figure 13. Fatigue damage of different gears under different mean wind speeds and the same turbulence scale: (a) $I_u = 10\%$; (b) $I_u = 20\%$; and (c) $I_u = 30\%$.

The sun gear damage is larger than that of the other parts, which is due to its large torque as a result of the low rotational speed compared to the gears at High Speed Intermediate Stage (HSIS) and High Speed Stage (HSS). Therefore the force in the planetary stage is larger than in the other parts. There are also three contact points in a sun gear (contacts with the three planetary gears), therefore it has a higher damage risk than the planetary gears. To further investigate sun gear fatigue damage variation tendency under different external environments, Figure 14 shows the calculation result for a sun gear when the mean wind speeds range from 4 m/s to 25 m/s and with turbulences changing from 10% to 30%. It is observed that when the mean wind speed is above 13 m/s, the fatigue damage increases quickly compared to the case of wind speed below the rated range. The magnitude of the fatigue damage is maintained for wind speeds above 13 m/s. and the damage starts to decrease when the mean wind speed is approaching 25 m/s. The damage variation tendencies for different turbulent scales are observed to be similar.

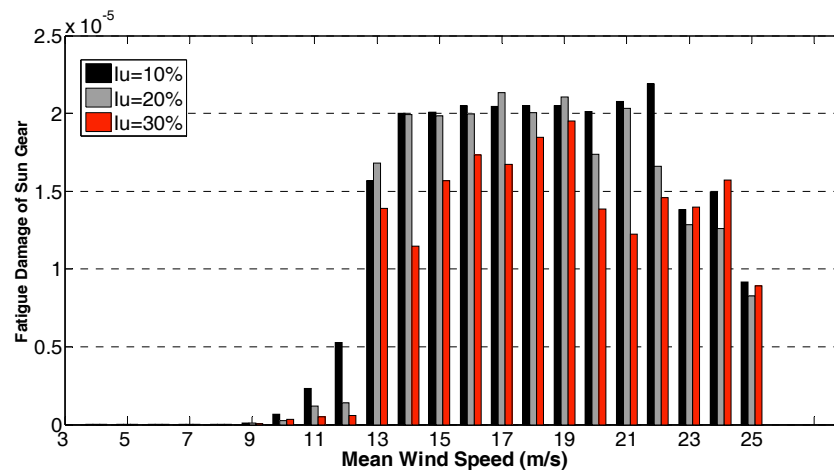


Figure 14. Fatigue damage of a sun gear.

From Figure 14, it is also observed that damages to the sun gear due to wind speeds with 30% turbulence intensity are lower compared to the cases with 10% and 20% turbulence intensity. The reason for this can be explained by Figures 11 and 12. Wind turbulences of 10% or 20% at wind speeds above the rated range cause a high probability of large mean bending stress and also large bending stress amplitude. These lead to further high stress cycles of large bending stress amplitude after Goodman correction, which results in significant damage to the gear, while for the case of wind speeds with 30% wind turbulence, the probability of appearance of large bending stress amplitudes is low which is due to the WT shutting down because the wind speeds are out of the operational range, that is either lower than the cut-in wind speed or higher than the cut-out wind speed. Essentially high bending stresses amplitude have more significant impact on fatigue damage than low bending stress amplitude. Therefore, 10% or 20% wind turbulences lead to higher sun gear damage than 30% wind turbulence. However, it should be pointed out that the result obtained here is by assuming that the WT has an instantaneous response to external excitation (wind speed variation). Lags in response of WT to transient wind speed variations may potentially expose the machine to high amplitude transient loads or bending stresses that may increase its damage risk. This transient effect is not considered in this paper and is a topic that may be worthy of future research.

6. Using SCADA Data for Long Term Damage Quantification

As shown in the previous sections, short-term damage is calculated by defining an average wind speed and turbulence intensity and simulation of gearbox dynamics. WT SCADA data is characterized by its low data sampling rates whereby only the average wind speed and the maximum, and minimum wind speed in ten minutes are recorded. Therefore, a statistical method is used to estimate the standard deviation of ten minutes' wind speed and then the turbulence intensity. The equation below is used [35]:

$$\sigma_u = \sqrt{\frac{(v_{\max} + v_{\min} - 2v_{\text{mean}})^2 + (v_{\max} - v_{\min})^2}{12}} \quad (17)$$

$$I = \frac{\sigma_u}{\bar{U}} \quad (18)$$

Wind speed data within the ten minutes being considered are taken as a sample data set with known mean, maximum and minimum values to derive the standard variation. Equation (17) is derived by transforming the median wind speed into mean wind speed referring to the formula given in [32]. Therefore, mean wind speed and turbulence intensity are two necessary parameters for short term gearbox damage prediction, which can be calculated as shown in the previous sections.

Long-term damages are quantified by summing up subsequent 10 min short-term damages which is illustrated in Figure 15.

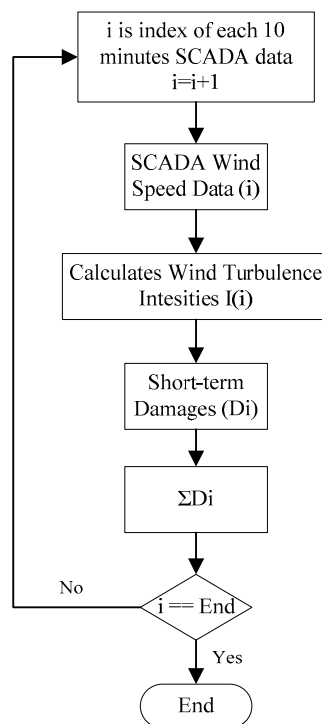


Figure 15. Procedure of long-term fatigue damage quantification by SCADA data.

The gearbox being analyzed is a WT three stage gearbox. It suffered a catastrophic failure on the sun gear of the planetary stage. The parallel stage showed no obvious damage. The failure is shown in Figure 16. Nearly all the teeth of the sun gear are broken. In some areas, an obvious fatigue stress zone is observed, which is highlighted in the figure. SCADA data from this gearbox is extracted for fatigue analysis.



Figure 16. WT gearbox sun gear of planetary stage teeth broken failure.

Although the SCADA data used here was not recorded from the first date when the WT was operating, the cumulative damage calculation is still validated as linear damage theory assumes that fatigue damage due to different stress levels are independent of each other and it can be linearly accumulated. The nine months SCADA data recorded before the WT failed are divided into three sections. Each section contains three months of SCADA data, which are further used to calculate the WT fatigue damage. The wind speed data are analyzed and shown in Figure 17. The short-term damage of each ten minute period is indexed by the mean wind speed and the calculated wind turbulence intensities within this period. The corresponding wind data statistical results are shown in Table 3 and in Figure 17. Table 3 shows the frequency of the mean wind speed exceeding 10 m/s and the turbulence intensity larger than 15% in subsequent period intervals before failure. The accumulative fatigue damage of the three section periods for different components of a gearbox are shown in Figure 18.

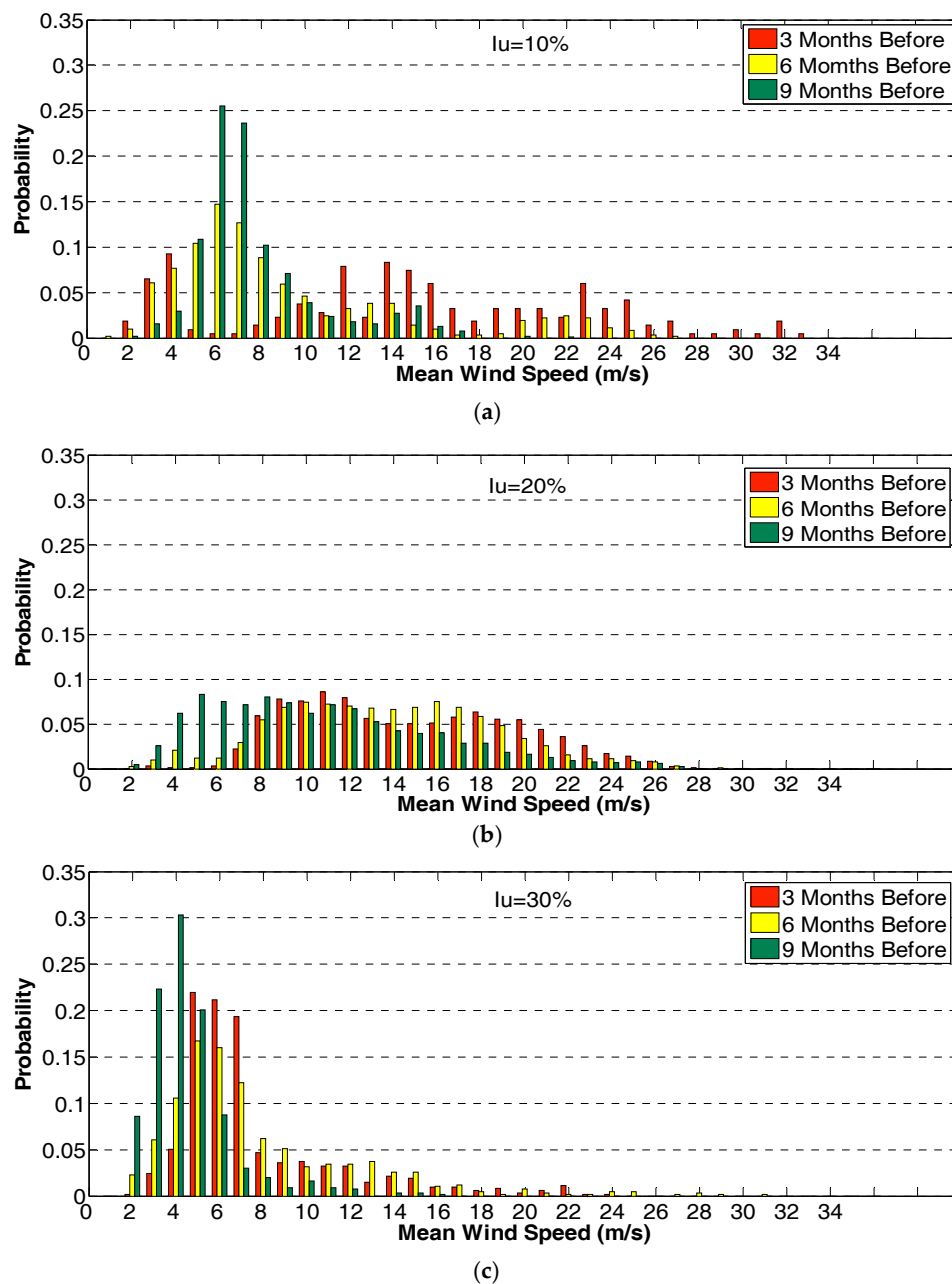
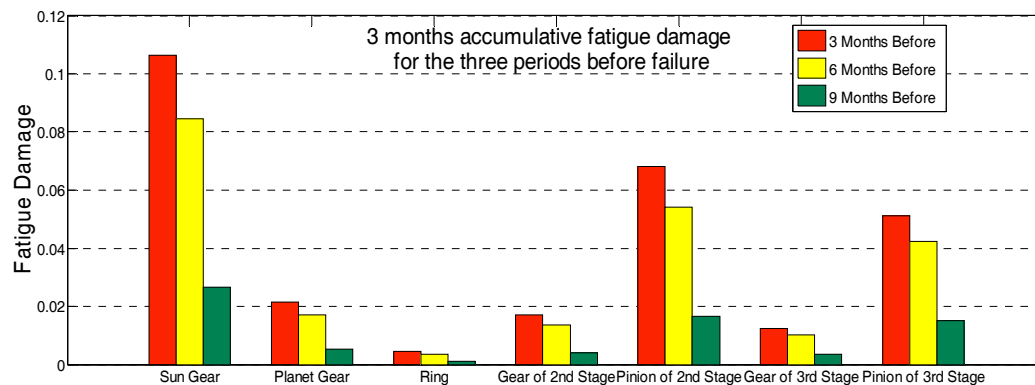


Figure 17. Distribution of mean wind speeds of different periods recorded by SCADA with different turbulence intensity: (a) 10%; (b) 20% and (c) 30%.

Table 3. Wind speed data of SCADA analysis.

Mean Wind Speed & Turbulence Intensity	June 2006–September 2006	September 2006–December 2006	December 2006–March 2007
$V_{\text{mean}} \geq 10 \text{ m/s}$	2481	6118	7428
$I_u \geq 15\%$	9078	10,175	11,121

**Figure 18.** The accumulative fatigue damage of three months at different periods.

Comparing the fatigue damage of different components, it shows that the sun gear damage is greater than that of the other components. For the second and third stages of the gearbox, their pinions are more vulnerable than gears. This agrees with the conclusion obtained in the short-term damage calculation. Comparing the damages accumulated for the three periods, the components' damages in the latest three months are larger than that in the other two periods. The smallest damages are observed for the earliest three months periods (nine months before). The damage may be due to the difference of the wind speed and turbulence scale distribution as shown in Figure 16.

High occurrence probability of high mean wind speed ($\geq 10 \text{ m/s}$) is observed for the turbulence scale of 10% and 20% during the three (December 2006–March 2007) and six (September 2006–December 2006) months before period. According to the short-term damage calculation results when the mean wind speed is above 10 m/s the damage to the gearbox increases significantly. This leads to the high damage estimated for the two periods. In addition, the turbulence intensities are also increasing, which further causes serious damages to the gearbox. As observed in Figure 18, the accumulative fatigue damage of the sun gear for the latest three months period is higher than 0.1. The total cumulative damage of nine months reached 0.2, which increases the gearbox failure probability. As the SCADA data used here is not recorded from the first date when the WT was operating, the cumulative damage value is lower than 1, but the trend shows significant damage during the six and three months before failure, which accounts for 20% of the whole service life.

7. Conclusions

A long-term fatigue damage assessment method of WTs based on practical SCADA data is developed in this paper. Short-term fatigue damage of WT gearboxes which considers the impact of turbulence is firstly investigated. The main shaft mechanical torques under turbulent wind speeds as external excitations are obtained for gear mechanics. A three-stage gearbox multibody dynamic model which considers time-varying meshing stiffness is established to study the gears' stress dynamics. Gear stress cycle distributions and fatigue damages are then evaluated by a rain-flow counting method and Palmgren-Miner theory. To consider the impacts of mean stress level the Goodman linear equation is used to revise the stresses S-N curve. A long-term fatigue damage quantification approach using SCADA data is finally proposed. By referring to the mean, maximum and minimum wind speeds in

the SCADA data, wind turbulence intensities are calculated for each 10 min time interval. Then fatigue damage is accumulated subsequently for long-term damage quantification.

The quantification results indicate that for the current design, the most vulnerable components of WT gearbox are the sun gears. For the parallel stages, pinion damages are higher than those of gears. Special consideration to protect or avoid fatigue damage of sun gears and pinions should be carried out during the design stage. WT gearboxes show different sensitivity to different mean wind speeds. Higher damage should be expected when the WT is operating under wind conditions that being with mean wind speed above 10 m/s. Although with low data sampling rate, by assuming that wind speed distribution obey a statistical law SCADA data can be used to quantify gearbox long-term fatigue damage. The analysis result of nine months of SCADA data shows a prominent gearbox damage tendency, which can be used for WT gearbox monitoring. The approach is capable of effectively presenting the performance degradation of gearboxes' different components due to wind speed variation. The accuracy of this method is determined by the short-term fatigue damage calculation which is affected by the variation of material/structural parameters and random external excitation situations. Further validation and increased sample cases will be helpful to improve the accuracy of this approach. In any case, the quantification approach proposed here provides a useful tool for wind farm maintenance prognosis.

Acknowledgments: This is a research work funded by National Natural Science Foundation of China (Grant No. 51505225), Natural Science Foundation of Jiangsu Province (BK20131350), The Fundamental Research Funds for the Central Universities, (No. 30915011324), Jiangsu Top Six Talent Summit Fund (ZBZZ-045).

Author Contributions: All the authors contributed to the theoretical model development, data analysis and interpretation of the comparison results.

Conflicts of Interest: The authors declare no conflict of interest.

References

1. Tavner, P. *Offshore Wind Turbine Reliability, Availability and Maintenance*, 1st ed.; Institution of Engineering and Technology (IET): London, UK, 2012.
2. Jin, X.; Ju, W.; Zhang, Z.; Guo, L.; Yang, X. System safety analysis of large wind turbines. *Renew. Sustain. Energy Rev.* **2016**, *56*, 1293–1307. [[CrossRef](#)]
3. Beganovic, N.; Söffker, D. Structural health management utilization for lifetime prognosis and advanced control strategy deployment of wind turbines: An overview and outlook concerning actual methods, tools, and obtained results. *Renew. Sustain. Energy Rev.* **2016**, *64*, 68–83. [[CrossRef](#)]
4. Cao, M.; Qiu, Y.; Feng, Y.; Wang, H.; Li, D. Study of Wind Turbine Fault Diagnosis Based on Unscented Kalman Filter and SCADA Data. *Energies* **2016**, *9*, 847–865. [[CrossRef](#)]
5. Hyers, R.W.; McGowan, J.G.; Sullivan, K.L.; Manwell, J.F.; Syrett, B.C. Condition Monitoring and Prognosis of Utility Scale Wind Turbines. *Energy Mater.* **2006**, *1*, 187–203. [[CrossRef](#)]
6. Nejad, A.R.; Odgaard, P.F.; Gao, Z.; Moan, T. A prognostic method for fault detection in wind turbine drive train. *Eng. Fail. Anal.* **2014**, *42*, 324–336. [[CrossRef](#)]
7. Lau, B.C.P.; Ma, E.W.M.; Pecht, M. Review of offshore wind turbine failures and fault prognostic methods. In Proceedings of the Prognostics and System Health Management (PHM), Beijing, China, 23–25 May 2012.
8. International Organization for Standardization. *ISO 6336-1: Calculation of Load Capacity of Spur and Helical Gears—Part I: Basic Principles, Introduction and General Influence Factors*; International Organization for Standardization: Geneva, Switzerland, 2006.
9. International Electrotechnical Commission. *IEC 61400-4: Wind Turbines—Part 4: Standard for Design and Specification of Gearboxes*; International Electrotechnical Commission: Geneva, Switzerland, 2012.
10. Nejad, A.R.; Gao, Z.; Moan, T. On long-term fatigue damage and reliability analysis of gears under wind loads in offshore wind turbine drivetrains. *Int. J. Fatigue* **2014**, *61*, 116–128. [[CrossRef](#)]
11. Dong, W.; Xing, Y.; Moan, T.; Gao, Z. Time domain-based gear contact fatigue analysis of wind turbine drivetrain under dynamic conditions. *Int. J. Fatigue* **2013**, *48*, 133–146. [[CrossRef](#)]
12. Nejad, A.R.; Gao, Z.; Moan, T. Fatigue Reliability-Based Inspection and Maintenance Planning of Gearbox Components in Wind Turbine Drivetrains. *Energy Procedia* **2014**, *53*, 248–257. [[CrossRef](#)]

13. Wang, L.; Shen, T.; Chen, C.; Chen, H. Dynamic reliability analysis of gear transmission system of wind turbine in consideration of randomness of loadings and parameters. *Math. Probl. Eng.* **2014**, *2014*, 1–10. [[CrossRef](#)]
14. Peeters, J.L.; Vandepitte, D. Analysis of internal drive train dynamics in a wind turbine. *Wind Energy* **2006**, *9*, 141–161. [[CrossRef](#)]
15. Zhu, C.; Chen, S.; Liu, H.; Huang, H.; Li, G.; Ma, F. Dynamic analysis of the drive train of a wind turbine based upon the measured load spectrum. *J. Mech. Sci. Technol.* **2014**, *28*, 2033–2040. [[CrossRef](#)]
16. Lin, J.; Parker, R.G. Mesh stiffness variation instabilities in two-stage gear systems. *J. Vib. Acoust.* **2002**, *124*, 68–76.
17. Qiu, Y.; Xu, Y.; Li, J.; Feng, Y.; Yang, W.; Infield, D. Wind Turbulence Impacts to Onshore and Offshore Wind Turbines Gearbox Fatigue Life. In Proceedings of the 3rd Renewable Power Generation Conference, Naples, Italy, 24–25 September 2014.
18. Fernandes, P.J.L. Tooth Bending Fatigue Failures in Gears. *Eng. Fail. Anal.* **1996**, *3*, 219–225. [[CrossRef](#)]
19. Aberšek, B.; Flašker, J.; Glodež, S. Review of mathematical and experimental models for determination of service life of gears. *Eng. Fract. Mech.* **2004**, *71*, 439–453. [[CrossRef](#)]
20. Kramberger, J.; Šraml, M.; Potrč, I.; Flašker, J. Numerical calculation of bending fatigue life of thin-rim spur gears. *Eng. Fract. Mech.* **2004**, *71*, 647–656. [[CrossRef](#)]
21. International Electrotechnical Commission. *IEC61400-1, Wind turbines-Part 1: Design Requirements[S]*, 3rd ed.; International Electrotechnical Commission: Geneva, Switzerland, 2005.
22. Von, K.T. Progress in the Statistical Theory of Turbulence. *Proc. Natl. Acad. Sci. USA* **1948**, *34*, 530–539.
23. Bossanyi, E.A. *GH Bladed Version 3.83 Theory Manual*; Document 282/BR/009 ISSUE 013; Garrad Hassan and Partners Limited: Bristol, UK, 2005.
24. Liang, X.; Zuo, M.J.; Hoseini, M.R. Vibration signal modeling of a planetary gear set for tooth crack detection. *Eng. Fail. Anal.* **2015**, *48*, 185–200. [[CrossRef](#)]
25. Parker, R.G.; Agashe, V.; Vijayakar, S.M. Dynamic response of a planetary gear system using a finite-element contact mechanics model. *J. Mech. Des.* **2000**, *122*, 304–310. [[CrossRef](#)]
26. Kahraman, A.; Kharazi, A.; Umrani, M. A deformable-body dynamic analysis of planetary gears with thin rims. *J. Sound. Vib.* **2003**, *262*, 752–768. [[CrossRef](#)]
27. Yuksel, C.; Kahraman, A. Dynamic tooth loads of planetary gear sets having tooth profile wear. *Mech. Mach. Theory* **2004**, *39*, 695–715. [[CrossRef](#)]
28. Fakhfakh, T.; Chaari, F.; Haddar, M. Numerical and experimental analysis of a gear system with teeth defects. *Int. J. Adv. Manuf. Technol.* **2005**, *25*, 542–550. [[CrossRef](#)]
29. ISO 6336:3-1996. *Calculation of Load Capacity of Spur and Helical Gears—Part 3: Calculation of Tooth Bending Strength*; International Organization for Standardization: Geneva, Switzerland, 1996.
30. GB/T3480-1997. *Calculation Methods of Load Capacity for Involute Cylindrical Gears*; Chinese National Standard: Beijing, China, 1997.
31. Miner, M.A. Cumulative damage in fatigue. *J. Appl. Mech.* **1945**, *67*, 159–164.
32. Sun, L.; Liu, Y. Review of the Rain Flow Count Method and Its Application in Analysis of Vehicle Fatigue Damage. *Equip. Manuf. Technol.* **2012**, *12*, 35–36.
33. Marsh, G.; Wignall, C.; Thies, P.R.; Barltrop, N.; Incecik, A.; Venugopal, V.; Johanning, L. Review and application of Rainflow residue processing techniques for accurate fatigue damage estimation. *Int. J. Fatigue* **2016**, *82*, 757–765. [[CrossRef](#)]
34. Sendekyj, G.P. Constant life diagrams—A historical review. *Int. J. Fatigue* **2001**, *23*, 347–353. [[CrossRef](#)]
35. Hozo, S.P.; Djulbegovic, B.; Hozo, I. Estimating the mean and variance from the median, range, and the size of a sample. *BMC Med. Res. Methodol.* **2005**, *5*, 13. [[CrossRef](#)] [[PubMed](#)]

